Atom Indonesia

Journal homepage: http://aij.batan.go.id

A Novel Method for ^{57}Ni and ^{57}Co Production using Cyclotron-Generated Secondary Neutrons

H. Suryanto* **and I. Kambali**

Center for Radioisotope and Radiopharmaceutical Technology, National Nuclear Energy Agency, Puspiptek Area, Serpong, Tangerang Selatan 15314, Indonesia

ARTICLE INFO

Article history:
Received 1 November 2016
Received in revised form 12 September 2017
Accepted 20 February 2018

Keywords:
^{57}Ni
^{57}Co
Cyclotron
Secondary neutron
Nuclear medicine
TALYS code

ABSTRACT

^{57}Ni and ^{57}Co radioisotpes are used in the synthesis of radiopharmaceuticals, for research purposes, as well as radiotherapy in nuclear medicine due to its decay characteristics. In this research, ^{57}Ni and ^{57}Co were produced using secondary neutrons. The secondary neutrons employed in this investigation were generated by bombarding 11 MeV protons into a target system consisting of Havar® foil as a vacuum window, aluminum foil as an energy degrader, aluminum tube as a target holder and nickel foil as a target via (p,n), (n,n) and (n,2n) nuclear reactions. The TALYS-calculated data were used to understand the origin of the secondary neutrons. In this experiment, variable Ni target thicknesses of 75, 150 and 225 μm were irradiated with a fixed proton beam dose of 0.67 μAhr in order to study the dependence of the radioisotope yields on the target thickness. For the first time, ^{57}Ni and ^{57}Co radioisotopes were produced and observed experimentally following ^{58}Ni(n,2n)^{57}Ni → ^{57}Co nuclear reaction. Experimental results indicated that for 225-μm thick Ni target, the ^{57}Ni yield of 10.85 ± 3.29 μCi/μAhr and ^{57}Co yield of 6.04 ± 2.45μCi/μAhr were recorded after an hour cooling period. The resulted yields did not strongly depend on the target thickness. This proposed novel method is a promising method to obtain higher radioactivity yield in the production of ^{57}Ni and ^{57}Co radioisotopes.

INTRODUCTION

Nickel is a transition metal that has physical properties such as hard and tenacious, silvery-white lustrous with slight golden highlights. Nickel is a unique metal resistant to the action of alkaline and reacts slowly with a strong acid. In mechanical engineering nickel is often used for containers of concentrated sodium hydroxide solution. Over the past decades, nickel has become an important material in nuclear medicine. It can be used as a target material for the production of medical radioisotopes such as ^{57}Ni and ^{57}Co. Both radioisotopes are used in the synthesis of radiopharmaceuticals, research purposes, as well as radiotherapy in nuclear medicine due to its decay characteristics [1,2]. ^{57}Ni is a positron-emitting radioisotope (T½ = 35.6 h, $E_{\beta+}$ = 0.86 MeV, $I_{\beta+}$ = 35 %). It can be used for radiolabelling of Doxorubicin which is a potential radiopharmaceutical for PET imaging for evaluating the pharmacokinetic studies of anti-cancer drugs. On the other hand, ^{57}Co is a γ-emitting radioisotope (EC, T½ = 271 d, E_γ = 122.13 keV, I_γ = 85.6 %) that can be used as a label compound for radiotracer purposes and can also be used as a marker to estimate organ size and for in vitro diagnostic kits [2].

The short-lived ^{57}Ni and ^{57}Co radioisotopes can be produced directly by an energetic charged particles from a cyclotron accelerator. However, it may require higher energy particles to produce them via ^{58}Ni(p,d)^{57}Ni, ^{58}Ni(p,pn) ^{57}Ni, ^{56}Fe(^{3}He, 2n)^{57}Ni, ^{58}Ni(p,2p)^{57}Co, ^{62}Ni(p,2n + α)^{57}Co, and ^{64}Ni(p, 4n + α)^{57}Co nuclear reactions. The threshold energies for such reactions are 10.2 MeV, 12.4 MeV, 6.0 MeV, 8.31 MeV, 18.98 MeV, and 35.73 MeV respectively [1,2].

There has been limited literatures on the production of ^{57}Ni. Previous experimental research [3] suggested that ^{57}Ni radioisotope could be

*Corresponding author.
E-mail address: harisur@batan.go.id
DOI: https://doi.org/10.17146/aij.2018.872

produced by bombarding a 25-MeV helium-3 beam into a natural iron target, though the radioactivity yield was still relatively low (nearly 32 µCi/µAh). To the best of the authors knowledge, there has been no attempt to use secondary neutrons from proton-irradiated targets to produce ^{57}Ni radioisotope. Therefore it is essential to investigate such a method.

In this investigation, ^{57}Ni and ^{57}Co are produced using cyclotron generated-secondary neutrons by ^{58}Ni (n,2n)^{57}Ni → ^{57}Co nuclear reaction. To generate secondary neutrons as a neutron source, low energy charged particles (11 MeV proton) accelerated in a cyclotron is directed into a target system consisting of Havar® foil as a vacuum windows, aluminum as a degrader, aluminium target holder and nickel foils as a target via (p,n), (n,n) and (n,2n) nuclear reactions. The ^{57}Ni radioisotope is generated from nuclear reactions between ^{58}Ni and the secondary neutrons, while ^{57}Co radioisotope is formed following ^{57}Ni radioisotope decay. This production method is a novel method for producing ^{57}Ni and ^{57}Co radioisotopes, particularly the use of cyclotron to generate secondary neutrons. In addition, the results of this experimental production is confirmed with the TALYS code [4] and SRIM code [5] calculations as well as the available literatures. Both TALYS and SRIM codes have been widely employed in ion beam studies [6-10].

EXPERIMENTAL METHODS

SRIM and TALYS code calculations

The SRIM-2013 code [5] was employed to calculate the range and energy loss of proton in the targets of interest, including in natural copper (Cu) target for proton energy measurement, Havar window, aluminium (Al) degrader as well as natural Ni target. In the simulations, as many as 99,999 protons were irradiated into the targets at 90° incident angle with respect to the target surface. The calculated proton ranges were then used to confirm the experimental measurement of proton energy as well as to study the proton's depth of penetration in Ni target. Moreover the SRIM-calculated proton energy loss in Al degrader was also highlighted to understand the nature of proton stopping power in the material.

Calculations of (p,n), (n,n) and (n,2n) nuclear cross-sections and neutron production yields were carried out using the TALYS-1.8 code [4] for Havar, Al and Ni targets. The many state-of-the-art nuclear models are included to take into account of all main reaction mechanisms encountered in proton and neutron-induced nuclear reactions relevant for this investigation.

Proton energy measurement

The incident proton energy was measured using a stacked foil method similar to calibration curve method discussed elswhere [11-13]. In this experimental energy measurement, 8 copper (Cu) foils comprising of 1 foil measuring 40-µm thick and 7 Cu foils measuring 20-µm thick each, were pressed together and then bombarded with the incoming proton beams at a dose of 0.67 µAhr. The gamma rays produced from ^{65}Cu(p,n)^{65}Zn nuclear reaction were measured using a portable gamma ray spectroscopy system (made by Amptek, USA) consisting of an NaI(Tl) detector and portable Multi Channel Analyzer (MCA) (Type MCA8000A, serial number 2278). The relative intensity of the measured gamma ray was then plotted against the proton's depth of penetration. The proton energy (E_p) was determined by taking into account of the proton threshold energy (E_{th}) for ^{65}Cu(p,n)^{65}Zn nuclear reaction (calculated using the TALYS 1.8 code), and the energy in which proton beam can still activate the Cu foils (E_{tdp}). The formula can be expressed as follows:

$$E_p = E_{th} + E_{tdp} \quad (1)$$

Nickel target irradiation and measurement

The target used in this experiment was a natural nickel with a purity of 99.9 % and a thickness of 25 µm each. The target was purchased from Goodfellow, England. Natural Ni consists of five stable isotopes: ^{58}Ni (68.27 %), ^{60}Ni (26.10 %), ^{61}Ni (1.13 %), ^{62}Ni (3.59 %), and ^{64}Ni (0.91 %). In this experiment, there were three sets of target thicknesses used in this experiment, namely 75, 150 and 225 µm respectively, where each set of the target was composed of stacked Ni foils with a thickness of 25 µm each. Each set of the foils was then irradiated with 11-MeV proton beam for 2 minutes. The beam current was kept constant at 20 µA, resulting in an integrated current dose of 0.67 µA.hr. The experimental setup is shown in Fig. 1, which comprises of a 25-µm Havar foil, a 70-µm aluminum degrader, Ni target and a target holder made of aluminum.

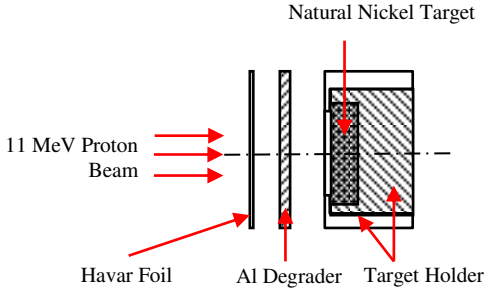

Fig. 1. Experiment setup for target irradiation.

After the end of the irradiations, and an appropriate cooling time, the targets were removed, and the gamma rays emmited from the activated targets were measured using a portable gamma ray spectrometer. The gamma ray spectrometer employed in this investigation consisted of NaI(Tl) detector which was connected to a portable multi channel analyzer (MCA). The portable MCA used herein was a typical MCA8000A made by Amptek USA with a serial number of 2278. The spectrometer system was calibrated using multiple gamma rays from Co-60 (Eγ = 1.17 and 1.33 MeV), Cs-137 (Eγ = 0.662 MeV) and Ir-192 (Eγ = 0.308; 0.317; 0.468; 0.604 and 0.612 MeV) radioactive sources.

RESULTS AND DISCUSSION

Origin of secondary neutrons

In this investigation, there are various different secondary neutron sources in the target system as a result of the proton irradiation of Havar window, aluminum degrader, aluminum holder and Ni target.

Havar window

Havar foil, which comprises of cobalt (42.5 %), chromium (20 %), iron (18.1 %), nickel (13 %), tungsten (2.8 %), molybdenum (2 %), manganese (1.6 %), carbon (0.2 %), beryllium (0.04 %), and some other trace elements, is one of the neutron sources found in the target system. The metal alloy has been an interesting material in medical radionuclide production studies [14-16]. The 11-MeV proton beams produced by the cyclotron hit the 50-µm Havar foil, which result in ^{56}Fe(p,n)^{56}Co nuclear reaction as theoretically calculated and experimentally observed in previous studies [17-20]. Nuclear reactions between the 11-MeV proton beams and the rest of the Havar's individual atoms were not experimentally observed, though they could potentially generate secondary neutrons at low neutron fluxes. The TALYS-calculated data of neutron cross-sections and production yields for proton-Havar and neutron-Havar interactions are given in Fig. 2(a) and 2(b) respectively.

It can be seen from Fig. 2(a) that individual atoms such as Fe, Cr, Mo, Mn could potentially give rise to the number of secondary neutrons when an 11-MeV proton beam is bombarded to Havar foil since their (p,n) nuclear cross-sections are significantly high (over 300 mbarn), whereas secondary neutrons generated from proton-irradiated Ni atoms are expectedly low since its nuclear cross-section is theoretically 7.69 mbarn. The high nuclear cross-sections for proton-impinged Fe, Cr, Mo, Mn atoms result in the high secondary neutron production yield as shown in Fig. 2(a) inset.

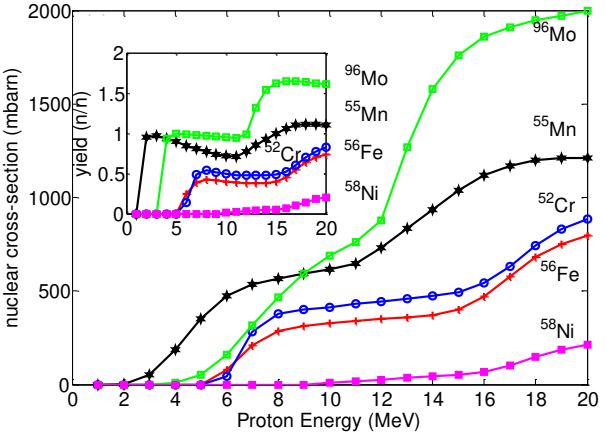

(a)

Fig. 2(a). Cross-sections of (p,n) nuclear reactions and secondary neutron production yield (inset) for individual atoms in Havar window as a function of proton energy.

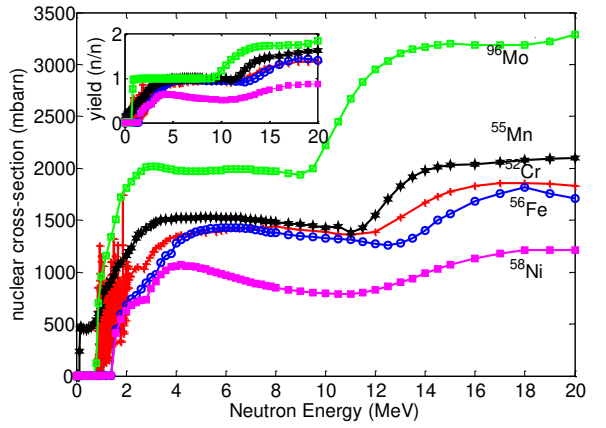

(b)

Fig. 2(b). Cross-sections of (n,n) nuclear reactions and secondary neutron production yield (inset) for individual atoms in Havar window as a function of neutron energy.

For (n,n) nuclear reactions, high nuclear cross-sections are evident for all individual Havar atoms (Fig. 2(b)), which eventually increase the number of secondary neutrons produced by the interactions. It should be noted that most secondary neutrons generated by (n,n) reactions are due to interactions between fast neutrons (E_n > 1 MeV) and the individual Havar's atoms. Moreover, the neutron production yield becomes greater than 1 at neutron energies greater than 10 MeV for Mo, Mn, Cr and Fe atoms as seen in Fig. 2(b) inset.

Aluminum degrader

As an energy degrader, the Al foil experiences bombardment by the incoming proton beam as well as secondary neutrons generated from proton-irradiated Havar window. As a result, secondary neutrons from these typical interactions are overwhelmingly produced and eventually hit the prepared Ni target. The TALYS-calculated cross-sections and neutron production yield for (p,n) and (n,n) reactions are shown in Fig. 3, which indicates that nuclear cross-sections are higher for (n,n) reaction compared to (p,n) reaction. For 8.2-MeV protons, the (p,n) nuclear cross-section is 78.9 mbar whereas for 11-MeV neutrons the (n,n) nuclear cross-section is 786 mbarn. The (n,n) cross-section is even maximum (934 mbarn) at neutron energy of 6.4 MeV. In general, the neutron production yield is also higher for (n,n) reaction (Fig. 3, inset). Note that in these calculations, the nuclear cross-sections shown in the figures are the total cross-sections derived from both (n,n) and (n,2n) nuclear reactions.

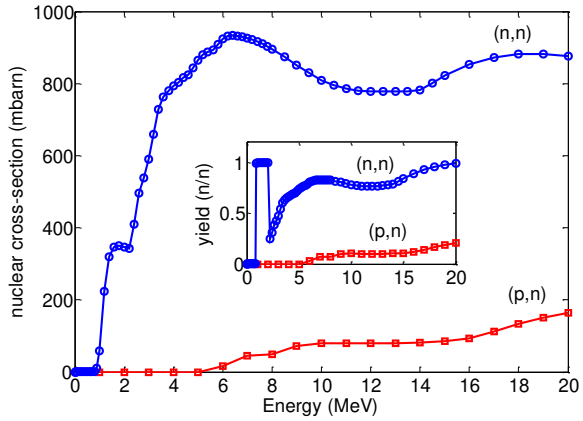

Fig. 3. Cross-sections of (p,n) and (n,n) nuclear reactions as well as secondary neutron production yield (inset) for Al degrader.

Aluminum holder

Aluminum holder used to house the Ni target in the target system is potentially hit by the incoming proton beam as well as neutron beams. The nuclear reaction occuring here is very similar to what happens to the Al degrader; thus the number of neutrons generated in the target system increases further.

Nickel target

After passing through the Havar window and Al energy degrader, the 11-MeV proton beams experience energy loss as a result of their interactions with Al atoms. Based on the SRIM code calculations and experimental results, as much as 2.8 MeV is lost during the protons – Al degrader interactions. As a result, 8.2-MeV protons irradiate the Ni target in this experiment. Apart from (p,n) nuclear reaction, (n,n) nuclear reaction also potentially occurs when the 8.2-MeV proton beam is directed onto the Ni target. According to the TALYS-calculated results for Ni(p,n) nuclear reaction, high nuclear cross-sections are evident for particularly ^{60,61,62,64}Ni atoms at proton energy of 8.2 MeV (see Fig. 4(a)). Surprisingly, the cross-section of ^{58}Ni(p,n) nuclear reaction is the lowest among the other Ni isotopes, whereas ^{64}Ni has the highest nuclear cross-section, and thus it also has the highest neutron production yield compared to the other Ni isotopes (Fig. 4(a), inset). In the proton energy range between 3 and 8.2 MeV, the neutron production yield for ^{64}Ni levels off at 1 neutron per 1 incoming proton, though the yield increases to greater than 1 for higher incoming proton energy.

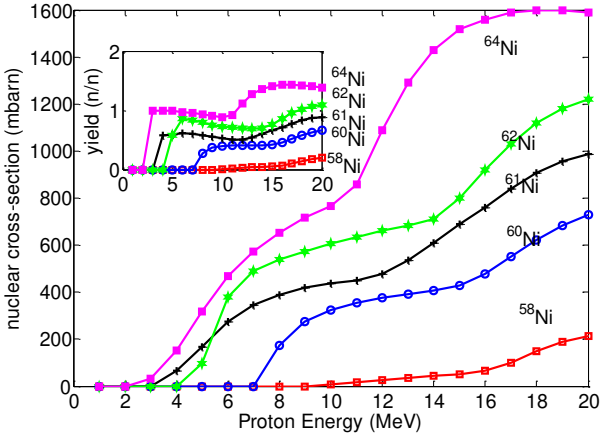

(a)

Fig. 4(a). Cross-sections of (p,n) nuclear reactions and secondary neutron production yield (inset) for individual atoms of Ni target.

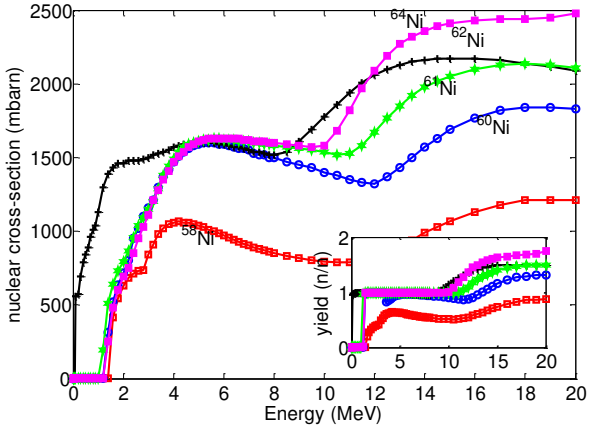

(b)

Fig. 4(b). Cross-sections of (n,n) nuclear reactions and secondary neutron production yield (inset) for individual atoms of Ni target.

Similar nuclear cross-section trend is also observed for (n,n) nuclear reactions of Ni isotopic target in which ^{58}Ni has the lowest cross-section compared to the other Ni isotopes, though the cross-section is relatively high (over 700 mbarn) for neutron energies greater than 3 MeV (Fig. 4(b)). In this instance, ^{64}Ni also has the highest nuclear cross-section and neutron production yield among others (Fig. 4(b), inset).

Incoming proton energy

In the proton energy measurement, a ^{65}Cu(p,n)^{65}Zn nuclear reaction takes place as the proton beams hit the Cu target. The resulting ^{65}Zn radionuclide emits gamma ray at 1.115 MeV with a half life of 245 days. The gamma ray spectrum of ^{65}Zn radionuclide measured using the portable gamma ray spectrometer is shown in Fig. 5 for different depth of proton penetration. As can be observed in the figure, the gamma ray intensity drops with increasing depth of penetration. The experimental results also indicate that the incident proton beam is able to penetrate Cu target at a depth of up to 100 µm (Fig. 5, inset). The 100 µm depth of penetration corresponds to the proton energy of 6 MeV. Note that the proton beam is considered being completely stopped when the 1.115-MeV gamma ray intensity equals to the background counts (nearly 1 % of the gamma ray maximum intensity).

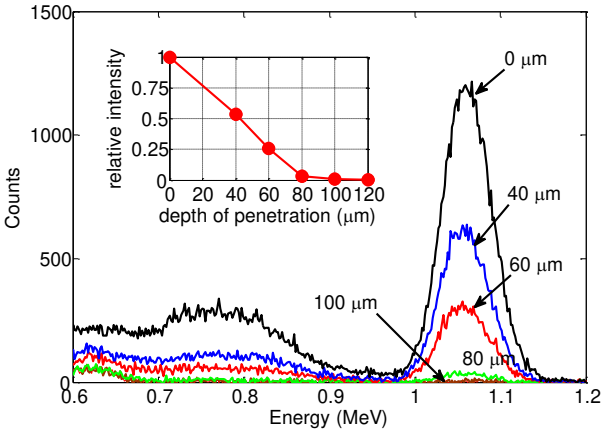

Fig. 5. Gamma ray spectrum of ^{65}Zn for different proton's depth of penetration, recorded using the Amptek-portable gamma ray spectroscopy system. The gamma ray relative intensity as a function of the proton's depth of penetration is given in the inset.

By taking the threshold energy for ^{65}Cu(p,n)^{65}Zn nuclear reaction into account (E_{th} = 2.2 MeV as calculated using the TALYS code), and by applying equation (1) in the energy determination, the proton energy was found to be 8.2 MeV. This proton energy is then employed in the ^{57}Ni radioisotope production highlighted in this report.

Havar and aluminum spectra

Gamma rays emitted by the Havar and aluminum energy degrader is shown in Fig. 6. For Havar spectrum, there are 2 pronounced peaks at 0.847 and 1.238 MeV which belongs to ^{56}Co radionuclide. ^{56}Co radionuclide is produced following proton bombardment of the Havar foil via ^{56}Fe(p,n)^{56}Co nuclear reaction. In addition, another significant peak at 0.511 MeV can be easily identified, which corresponds to the annihilation peak. The pair production process occurring when the 1.238 MeV gamma ray passes through or near the nucleus field of the detector is presumably responsible for the emerging peak at 0.511 MeV as discussed previously [15].

For aluminum spectrum shown in Fig. 6 (inset), there is only 1 distinguished peak at gamma ray energy of 0.844 MeV. The peak is presumably due to gamma ray emitted by ^{27}Mg following ^{27}Al (n,p) ^{27}Mg nuclear reaction. In theory, another radioactive isotope, ^{27}Si is produced as a result of proton-irradiated Al via ^{27}Al(p,n)^{27}Si nuclear reaction. However, the ^{27}Si peak is not observed in the spectrum since its half life is very short (4.2 second).

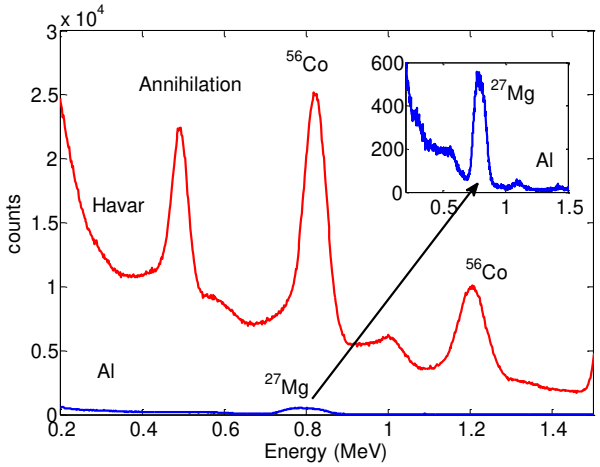

Fig. 6. Gamma ray spectrum of Havar foil (red line) and Al degrader (blue line). The aluminum spectrum is also shown in the inset for better analysis.

From the observed Havar and Al spectrum, it is clear that secondary neutrons are generated from the proton irradiation. Thus these secondary neutrons are expected to further activate the surrounding materials, particularly the natural nickel target investigated in this research.

Nickel spectra

As the secondary neutrons hit the natural nickel target, neutron-induced nuclear reaction occurs, and this occurance can be detected from the gamma ray spectrum recorded in the gamma ray

spectroscopy system. Experimental results indicate that a very strong peak at 0.511 MeV is observed as can be seen in Fig. 7. The annihilation peak is most likely due to ^{58}Ni(n,2n)^{57}Ni nuclear reaction, in which the produced ^{57}Ni emits positron. Subsequently, the positron annihilates into 2 gamma rays at 0.511 MeV as it collides with free electron. The annihilation peak here is comes from different process compared to the observed annihilation peak observed in Fig. 6. Another peak at 0.122 MeV is also recorded which corresponds to ^{57}Co peak, whereas a weak intensity is also detected between the ^{57}Co and ^{57}Ni peaks which belongs to the backscatters.

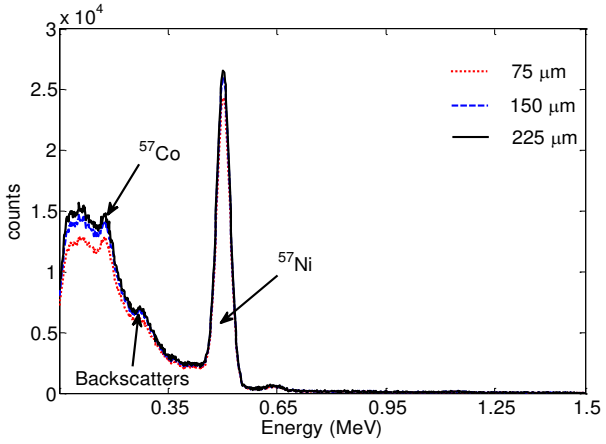

Fig. 7. Gamma ray spectrum of natural nickel target following 8.2-MeV proton bombardment at different target thicknesses.

Based on the experimental data of the three Ni target thicknesses irradiated with the same proton dose of 0.67 μA.hr, there is not much different in the gamma ray spectrum (see Fig. 7). This is due to the fact that secondary neutrons are responsible for the resulted ^{57}Ni and ^{57}Co radioisotopes. Unlike protons which experience high stopping powers as they pass through Ni target, neutrons can, in contrast, penetrate deep into and all over the natural Ni target since they have no net electric charge. Thus, for all varied Ni thicknesses (75, 150 and 225 μm thicks), generated radioactivities are nearly the same as shown in Table 1.

Table 1. Radioactivity yields of ^{57}Ni and ^{57}Co

Ni Target Thickness (μm)	Measured ^{57}Ni Yield (μCi/μAhr)	Measured ^{57}Co Yield (μCi/Ahr)
75	9.94 ± 3.15	5.22 ± 2.28
150	10.62 ± 3.26	5.78 ± 2.40
225	10.85 ± 3.29	6.04 ± 2.45

The radioactivities resulted from this investigation is low because of low proton beam dose employed in the experiment. Therefore, in order to increase ^{57}Ni and ^{57}Co yields, the irradiation parameters can be modified, including by: (i) replacing natural Ni target with enriched ^{58}Ni target, (ii) increasing the enriched ^{58}Ni target thickness, (iii) increasing proton energy (greater than 11 MeV), (iv) increasing proton beam dose (beam current and irradiation time), and (v) replacing aluminium degrader with berylium window to generate higher secondary neutron flux.

From the experimental data shown in Table 1, when the proton beam dose is increased to 50 μAhr, the expected ^{57}Ni and ^{57}Co radioactivities are 542.5 μCi and 302.0 μCi respectively for a 225 μm-thick Ni target. The expected ^{57}Ni radioactivity is, thus, nearly 17 times greater than the ^{57}Ni radioactivity previously obtained by Neirinckx [3]. In summary, the proposed novel method discussed in this report is a promising method to get higher radioactivity yield in the production of ^{57}Ni and ^{57}Co radioisotopes.

CONCLUSION

A novel method for ^{57}Ni and ^{57}Co Production using cyclotron-generated secondary neutrons have been conducted. The secondary neutrons are produced from proton-irradiated Havar window, aluminum foil, aluminum tube/holder and Ni target in the target system. In addition, the TALYS code calculations have also been employed to understand the origins of the secondary neutrons. Two pronounced radioactive elements, namely ^{57}Ni and ^{57}Co are experimentally produced following 8.2-MeV proton bombardment of the natural Ni targets. The target thickness variations, ranging from 75 and 225 μm, have shown no significant impact on the radioactivities. For the target thickness of 225 μm, the maximum radioactivities of ^{57}Ni and ^{57}Co are 10.85 ± 3.29 μCi/μAhr and 6.04 ± 2.45 μCi/μAhr respectively.

Further studies on optimum irradiation parameters as well as chemical separation of ^{57}Ni and ^{57}Co are suggested for better results.

ACKNOWLEDGMENT

The authours would like to acknowledge the World Academy of Sciences (TWAS) and National Nuclear Energy Agency (BATAN) for funding this research. Technical assistance by the cyclotron technicians at Dharmais Cancer Hospital in Jakarta also helps this research project to succeed.

REFERENCES

1. F.S. Al Saleh, K.S. Al Mugren and A. Azzam, Appl. Radiat. Isot. **65** (2007) 104.

2. M.U. Khandaker, K. Kim, M. Lee *et al.*, Nucl. Instrum. Methods Phys. Res., Sect. B **269** (2011) 1140.
3. R.D. Neirinckx, Int. J. Appl. Radiat. Isot. **28** (1977) 561.
4. A.J. Koning and D. Rochman, Nucl. Data Sheets **113** (2012) 2927.
5. J.F. Ziegler and M.D. Ziegler, Nucl. Instrum. Methods Phys. Res., Sect. B **268** (2010) 1818.
6. M. Eslami and T. Kakavand, Nucl. Instrum. Methods Phys. Res., Sect. B **329** (2014) 18.
7. H. Hofsäss, K. Zhang and A. Mutzke, Appl. Surf. Sci. **310** (2014) 134.
8. C. Yalçin, J. Phys. Conf. Ser. **590** (2015) 12050.
9. C.L. Fontana, C. Chen, M.L. Crespillo *et al.,* Nucl. Instrum. Methods Phys. Res., Sect. B **366** (2016) 104.
10. S. Kumar and P.K. Diwan, J. Radiat. Res. Appl. Sci. **8** (2015) 538.
11. I. Kambali and H. Suryanto, J. Eng. Tech. Sci. **48** (2016) 482.
12. I. Kambali, Parwanto, H. Suryanto *et al*., Physics Research International **2017** (2017) 1.
13. I. Kambali, Atom Indonesia **40** (2014) 129.
14. J.J. Martinez-Serrano and A. Diez de Los Rios, Health Phys. **107** (2014) 103.
15. H. Skliarova, M. Renzelli, O. Azzolini *et al.*, Thin Solid Films **591** (2015) 316.
16. M. Köhler and J. Konheiser, Appl. Radiat. Isot. **81** (2013) 268.
17. I. Kambali, H. Suryanto and Parwanto, Australas. Phys. Eng. Sci. Med. **39** (2016) 403.
18. M.J. Gladys, I. Kambali, M.A. Karolewski *et al.*, J. Chem. Phys. **132** (2010) 024714.
19. I. Kambali, D.J. O'Connor, M.J. Gladys *et al.*, Appl. Surf. Sci. **254** (2008) 4245.
20. I. Kambali, Makara J. Science **21** (2017) 125.